

Spin-Imbalance in a One-Dimensional Fermi Gas

Yean-an Liao^{1*}, Ann Sophie C. Rittner^{1*}, Tobias Paprotta¹, Wenhui Li^{1,†}, Guthrie B. Partridge^{1,‡}, Randall G. Hulet¹, Stefan K. Baur² & Erich J. Mueller²

¹*Department of Physics and Astronomy and Rice Quantum Institute, Rice University, Houston, TX 77251, USA.*

²*Laboratory of Atomic and Solid State Physics, Cornell University, Ithaca, NY 14853, USA.*

** These authors contributed equally to this work.*

[†] Permanent address: Centre for Quantum Technologies, National University of Singapore, 3 Science Drive 2, Singapore, 117543.

[‡] Present address: Laboratoire Charles Fabry de l'Institut d'Optique, UMR CNRS 8501, Palaiseau, France.

Superconductivity and magnetism generally do not coexist. Changing the relative number of up and down spin electrons disrupts the basic mechanism of superconductivity, where atoms of opposite momentum and spin form Cooper pairs. Nearly forty years ago Fulde and Ferrell¹ and Larkin and Ovchinnikov² proposed an exotic pairing mechanism (FFLO) where magnetism is accommodated by formation of pairs with finite momentum. Despite intense theoretical and experimental efforts, however, polarized superconductivity remains largely elusive³. Here we report experimental measurements of density profiles of a two spin mixture of ultracold ⁶Li atoms trapped in an array of one dimensional (1D) tubes, a system analogous to electrons in 1D wires. At finite spin imbalance, the system phase separates with an inverted phase profile in comparison to the three-dimensional case. In 1D we find a partially polarized core surrounded by wings composed of either a completely paired BCS superfluid or a fully polarized Fermi

gas, depending on the degree of polarization. Our observations are in quantitative agreement with theoretical calculations⁴⁻⁹ in which the partially polarized phase is found to be a 1D analogue of the FFLO state. This study demonstrates how ultracold atomic gases in 1D may be used to create non-trivial new phases of matter, and also paves the way for direct observation and further study of the FFLO phase.

The FFLO states are perhaps the most interesting of a number of exotic polarized superconducting phases proposed in the past 40 years. In the original concept of Fulde and Ferrell (FF), Cooper pairs form with finite centre of mass momentum¹. Larkin and Ovchinnikov (LO) proposed a related model where the superconducting order parameter oscillates in space². These two ideas are closely related, as the oscillating order parameter may be interpreted as an interference pattern between condensates with opposite centre of mass momenta. The spin density also oscillates in the LO model, leading to a build-up of polarization in the superconducting nodes. Thus the LO state can be considered a form of micro-scale phase separation with alternating superfluid and polarized normal regions. By including more and more momenta, subsequent theorists were able to evaluate the stability of ever more complicated spatial structures³.

Previous studies of superfluidity in fermionic atoms show that ultracold atoms are a powerful tool for investigating the emergent properties of interacting systems of many particles. While largely analogous to an electronic superconductor, the atomic systems feature tunable interactions. This extra degree of control has led to a number of unique experiments and conceptual advances. Furthermore, the absence of spin relaxation enables us to spin-polarize the atoms in order to explore the interplay between magnetism and superfluidity, with the potential to observe the FFLO phase. Unfortunately, theoretical calculations indicate that if an FFLO phase exists in three dimensional (3D) trapped gases, it will occupy an extremely small volume¹⁰.

Experiments in 3D show that the gas phase separates with an unpolarized superfluid core surrounded by a polarized shell¹¹⁻¹⁵, with no evidence for the FFLO phase. Here, we study a polarized Fermi gas in 1D, where theory predicts that a large fraction of the phase diagram is occupied by an FFLO-like phase (see Fig. 1a)⁵⁻⁹. In this 1D setting, the physics should be closest to that described by LO, where an oscillating superfluid order parameter coexists with a spin-density wave. Due to fluctuations, the order will be algebraic rather than long-ranged. The improved stability of FFLO-like phases in 1D can be understood as a “nesting” effect, where a single wavevector connects all points on the Fermi surface, allowing all atoms on the Fermi surface to participate in finite momentum pairing. In 3D, only a small fraction of these atoms are able to participate in finite momentum pairing. Similar enhancements are predicted for systems of lattice fermions and quasi-1D geometries^{7,16}.

Our work complements studies of astrophysical objects³ and solid state systems. Like our current experiment, the solid state experiments typically involve highly anisotropic materials – made up either of weakly coupled two-dimensional planes or 1D wires. Examples include the organic superconductor λ -(BETS)₂FeCl₄¹⁷ and the heavy fermion superconductor CeCoIn₅^{18,19}. Despite circumstantial evidence, FFLO states have not been conclusively observed in any solid state material.

Details of our experimental procedures are given in Methods and in Refs. 12 and 13. We create a mixture of the two lowest hyperfine levels of the ⁶Li ground state, the majority state $|1\rangle$, and the minority state $|2\rangle$. An array of 1D tubes is formed with a 2D optical lattice²⁰. There are several requirements for the system to be 1D. First, only the lowest transverse mode in each tube may be populated. This requires that both the thermal energy $k_B T$ and the 1D Fermi energy $\epsilon_F = N_1 \hbar \omega_z$ be small compared to the transverse confinement energy $\hbar \omega_\perp$. Here N_1 is the number of atoms in state $|1\rangle$ per 1D tube, and ω_z and ω_\perp are the axial and transverse confinement frequencies of an

individual tube. In our experiment the tube aspect ratio $\omega_{\perp}/\omega_z = 1000$ is much larger than $N_1 \sim 125$ for the central tube. Second, ε_F must be sufficiently larger than the bandwidth of the optical lattice to ensure that inter-tube coupling is small. In the non-interacting limit, this condition is equivalent to requiring that the Fermi surface be one-dimensional. A related condition is that the Josephson coupling between superfluids in neighbouring wells should be small. Prior analysis demonstrates that under these conditions the equation of state of the array of tubes reflects that of a single tube^{6,7}. We employ a lattice potential $V = V_0 \cos^2(kx) + V_0 \cos^2(ky)$, with $k = 2\pi/\lambda$ and $V_0 = 12 \varepsilon_r$, where x and y are two orthogonal radial coordinates, λ is the optical trap laser wavelength of 1064 nm, and $\varepsilon_r = \hbar^2 k^2 / 2m$ is the recoil energy. We tune an external magnetic field to the BCS side (890 G) of the broad 3D Feshbach resonance in ${}^6\text{Li}$ ^{21,22}, where the 1D interactions are strongly attractive^{23,24}. We determine the density distribution for each spin state from *in situ* images of the atoms in the lattice, and from these, extract the equation of state assuming hydrostatic equilibrium in each tube. Under this assumption, the 1D spatial density profile $n_{1,2}(z)$ can be expressed in terms of $\mu = \mu_0 - V(z)$, and $h = h_0$ where μ_0 and h_0 are the chemical potential and chemical potential difference at the centre of the tube, set by the total number of particles in the tube $N = N_1 + N_2$ and polarization $P = (N_1 - N_2)/N$; $V(z)$ is the axial confinement potential. In particular, the phase boundary between the fully paired and partially polarized regions in Fig. 1b occurs where the spin density $n_1(z) - n_2(z) = 0$, and the boundary between the fully and partially polarized phases corresponds to $n_2(z) = 0$.

Figure 2 shows column density profiles of state $|1\rangle$, state $|2\rangle$, and their difference, illustrating these phase boundaries. Column densities record the line-of-sight integrated densities through the centre of the cloud. As predicted by the phase diagram (Fig. 1), any given image has at most two of the three phases: the partially polarized region always lies at the centre of the trap, while the wings are fully paired at low P [see Fig. 2a) and fully polarized at high P (see Fig. 2c). This is distinctly different from a

polarized 3D gas where the centre is always fully paired. The critical polarization P_c is the boundary between these two behaviours [Fig. 2(b)], where the partially polarized region extends to the edge of the cloud. The column densities quantitatively agree with predictions from a finite temperature Bethe ansatz theory, where the only free parameter is temperature (see Methods for details). This theory predicts that the partially polarized phase is of the FFLO type⁵⁻⁹.

To extract the number of particles in the central tube we first integrate the column density images to produce a radial density $n_r(x) = \int n(x,y,z) dy dz$. We find that this radial density is well described by a functional form $n_r(x) = A (1 - x^2/b^2)^3$. As described in the methods section, the number of particles in the central tube is then $N_0 = (4 A \lambda^2)/(5 \pi b)$. From the column density plots, we extract the axial radii where the minority density and density difference vanish. Figure 3 shows these radii, normalized by $(N_0)^{1/2} a_z$, where $a_z = (\hbar/m\omega_z)^{1/2}$ is the harmonic oscillator length along the central tube. The critical polarization P_c corresponds to the crossing of these two radii: for $P < P_c$ the density difference vanishes before the minority density, while the opposite occurs for $P > P_c$. Our calculations show that the location of this crossing is highly temperature dependent, as can be seen from the inset to Fig. 3; for our experimental parameters at $T = 0$, $P_c = 0.15$ (see Methods for parameters). For $T > 200$ nK the fully paired wings are expected to be unobservable. The radii fit well to theory assuming $T = 130$ nK, corresponding to $T/T_F \approx 0.1$ in the lattice, where $T_F = \epsilon_F/k_B$ (see Methods). The difference data at low P and the minority at high P fit better to $T \sim 200$ nK. This may be an artefact of the relatively small signals in these cases that produces a systematic bias.

The observation of three distinct phases and the good quantitative agreement between experiment and theory is evidence for the presence of an FFLO phase in the 1D system. This is an example of an optical lattice-based quantum simulator that produces

a phase diagram of non-trivial quantum phases. In the future, we intend to fully characterize the partially polarized phase, to explicitly demonstrate its modulated order.

Methods Summary

We start from quantum degenerate, spin-imbalanced ${}^6\text{Li}$ Fermi gas in a single beam far-off resonance optical trap^{12,13}, loaded into a crossed beam optical dipole trap formed by a pair of retro-reflected beams propagating in the x and y directions. We turn on the 2D lattice by ramping up the optical trap laser power and rotating the polarization of the retro-reflected beams to create standing waves in two orthogonal directions. The intersection of the standing waves creates 1D tubes with an energy depth of $12 \epsilon_f$ in the central tube, with $\omega_{\perp,z} = (2\pi) (2 \times 10^5, 2 \times 10^2)$ Hz. At a global polarization $P \approx 0$, the total number of atoms is $\sim 2 \times 10^5$, giving a total number of atoms in the central tube of $N \sim 250$. For $P < 0.5$, the number of state $|1\rangle$ atoms in the central tube is 125 to within an estimated statistical and systematic uncertainty of 20%. The column densities of each state and their difference is obtained from two *in situ* polarization phase contrast images²⁵ taken in rapid succession and with different detuning. The temperature is determined by fitting the density of a balanced spin mixture to a Thomas-Fermi distribution²⁶ and is measured to be $T \sim 0.05 T_F$ before ramping up the 2D lattice. We find that the density profiles for a spin-imbalanced gas in the 2D lattice fit best to temperatures corresponding to $T/T_F \sim 0.1$ (see Methods).

Full Methods and any associated references are available in the online version of the paper at www.nature.com/nature.

1. Fulde, P. & Ferrell, R. A. Superconductivity in a Strong Spin-Exchange Field. *Phys. Rev.* **135**, A550–A563 (1964).
2. Larkin, A. I. & Ovchinnikov, Y. N. Inhomogeneous state of superconductors. *Sov. Phys. JETP* **20**, 762-769 (1965).

3. Casalbuoni, R. & Nardulli, G. Inhomogeneous superconductivity in condensed matter and QCD. *Rev. Mod. Phys.* **76**, 263–320 (2004).
4. Yang, K. Inhomogeneous superconducting state in quasi-one-dimensional systems. *Phys. Rev. B* **63**, 140511(R) (2001).
5. Orso, G. Attractive Fermi Gases with Unequal Spin Populations in Highly Elongated Traps. *Phys. Rev. Lett.* **98**, 070402 (2007).
6. Hu, H., Liu, X.-J. & Drummond, P. D. Phase Diagram of a Strongly Interacting Polarized Fermi Gas in One Dimension. *Phys. Rev. Lett.* **98**, 070403 (2007).
7. Parish, M. M., Baur, S. K., Mueller, E. J. & Huse, D. A. Quasi-One-Dimensional Polarized Fermi Superfluids. *Phys. Rev. Lett.* **99**, 250403 (2007).
8. Casula, M., Ceperley, D. M. & Mueller, E. J. Quantum Monte Carlo study of one-dimensional trapped fermions with attractive contact interactions. *Phys. Rev. A* **78**, 033607 (2008).
9. Kakashvili, P. & Bolech, C. J. Paired states in spin-imbalanced atomic Fermi gases in one dimension. *Phys. Rev. A* **79**, 041603 (2009).
10. Sheehy, D. E. & Radzihovsky, L. BEC-BCS crossover, phase transitions and phase separation in polarized resonantly-paired superfluids. *Annals of Physics* **322**, 1790–1924 (2007).
11. Zwierlein, M. W., Schirotzek, A., Schunck, C. H. & Ketterle, W. Fermionic Superfluidity with Imbalanced Spin Populations. *Science* **311**, 492–496 (2006).
12. Partridge, G. B., Li, W., Kamar, R. I., Liao, Y.-a. & Hulet, R. G. Pairing and Phase Separation in a Polarized Fermi Gas. *Science* **311**, 503–505 (2006).

13. Partridge, G. B. *et al.* Deformation of a Trapped Fermi Gas with Unequal Spin Populations. *Phys. Rev. Lett.* **97**, 190407 (2006).
14. Shin, Y.-I., Schunck, C. H., Schirotzek, A. & Ketterle, W. Phase diagram of a two-component Fermi gas with resonant interactions. *Nature* **451**, 689–693 (2008).
15. Nascimbene, S. *et al.* Collective Oscillations of an Imbalanced Fermi Gas: Axial Compression Modes and Polaron Effective Mass. *Phys. Rev. Lett.* **103**, 170402 (2009).
16. Zhao, E. & Liu, W. V. Theory of quasi-one-dimensional imbalanced Fermi gases. *Phys. Rev. A* **78**, 063605 (2008).
17. Uji, S. *et al.* Vortex Dynamics and the Fulde-Ferrell-Larkin-Ovchinnikov State in a Magnetic-Field-Induced Organic Superconductor. *Phys. Rev. Lett.* **97**, 157001 (2006).
18. Radovan, H. *et al.* Magnetic enhancement of superconductivity from electron spin domains. *Nature* **425**, 51–55 (2003).
19. Kenzelmann, M. *et al.* Coupled Superconducting and Magnetic Order in CeCoIn₅. *Science* **321**, 1652–1654 (2008).
20. Moritz, H., Stöferle, T., Günter, K., Köhl, M. & Esslinger, T. Confinement Induced Molecules in a 1D Fermi Gas. *Phys. Rev. Lett.* **94**, 210401 (2005).
21. Houbiers, M., Stoof, H. T. C., McAlexander, W. I. & Hulet, R. G. Elastic and inelastic collisions of ⁶Li atoms in magnetic and optical traps. *Phys. Rev. A* **57**, R1497–R1500 (1998).

22. Bartenstein, M. *et al.* Precise Determination of ${}^6\text{Li}$ Cold Collision Parameters by Radio-Frequency Spectroscopy on Weakly Bound Molecules. *Phys. Rev. Lett.* **94**, 103201 (2005).
23. Tokatly, I. V. Dilute Fermi Gas in Quasi-One-Dimensional Traps: From Weakly Interacting Fermions via Hard Core Bosons to a Weakly Interacting Bose Gas. *Phys. Rev. Lett.* **93**, 090405 (2004).
24. Fuchs, J. N., Recati, A. & Zwerger, W. Exactly Solvable Model of the BCS-BEC Crossover. *Phys. Rev. Lett.* **93**, 090408 (2004).
25. Bradley, C. C., Sackett, C. A. & Hulet, R. G. Bose-Einstein Condensation of Lithium: Observation of Limited Condensate Number. *Phys. Rev. Lett.* **78**, 985–989 (1997).
26. Kinast, J. *et al.* Heat Capacity of a Strongly Interacting Fermi Gas. *Science* **307**, 1296–1299 (2005).

Supplementary Information accompanies the paper on www.nature.com/nature

Acknowledgements EJM would like to thank Carlos Bolech and Paata Kakashvili for discussion of techniques for analyzing the data. Supported under ARO Award W911NF-07-1-0464 with funds from the DARPA OLE Program, and by the NSF, ONR, and the Welch (grant C-1133) and Keck Foundations.

Author's Contributions

Author Information Correspondence and requests for materials should be addressed to Randall G. Hulet (randy@rice.edu).

Methods

Preparation. We produce a quantum degenerate, strongly interacting, spin-imbalanced ${}^6\text{Li}$ Fermi gas using our previously published methods^{12,13}. Starting from a quantum degenerate gas of ${}^6\text{Li}$ in a single beam far-off resonance optical dipole trap, we control the relative population of two hyperfine states, $F = 1/2$, $m_F = 1/2$ (state $|1\rangle$) and $F = 1/2$, $m_F = -1/2$ (state $|2\rangle$), where F is the total spin and m_F is the projection along the quantization axis, by driving radio frequency sweeps between them at different power. The spin mixture is created in a uniform magnetic field at 765 G within the broad Feshbach resonance between states $|1\rangle$ and $|2\rangle$ centred at 834 G ^{21,22}. During evaporation, the field is adiabatically swept to 890 G, on the BCS side of the Feshbach resonance where the 3D scattering length $a_{3D} = -9200 a_0$ (a_0 is the Bohr radius). Atoms are evaporatively cooled by lowering the trap depth in the single beam optical trap. At the end of evaporation, we turn on a crossed-beam optical dipole trap formed by two orthogonal, retro-reflected laser beams, with elliptical laser beam waists ($1/e^2$ radii) of $54 \mu\text{m}$ by $236 \mu\text{m}$, with the beams propagating in the x - y plane and the long axes of the ellipses oriented along z . The polarization of each retro-reflected beam is controlled by liquid crystal variable retarders (LCVRs) and is perpendicular to that of the incident beam in the trap configuration. The trap depth is $0.5 \mu\text{K}$ with axial and the radial trapping frequencies of 50 and 153 Hz, respectively. We then turn on the optical lattice by simultaneously ramping up the laser power and rotating the polarization of each retro beam to be parallel to its corresponding incident beam, resulting in a 2D lattice of 1D tubes. The lattice turn-on time constants are 130 ms for intensity and 70 ms for polarization. Both turn-on trajectories are smooth error-function like trajectories, optimized to minimize heating. The final 1D lattice depth is $12 \epsilon_r$ ($\epsilon_r = 1.39 \mu\text{K}$) with radial and axial trapping frequencies in the central tube $(\omega_\perp, \omega_z) = (2\pi) (2 \times 10^5, 200)$ Hz. After waiting for 50 ms, we image the column densities of each state in the lattice. To a good approximation, the total number of atoms in the central tube, N_0 , decreases

linearly from 250 at $P = 0$ to 70 at $P = 1$. Correspondingly, the number of atoms in the central tube in state $|1\rangle$ is relatively constant at 125 for $P < 0.5$. Under these conditions $a_{\perp} = 1740 a_0$, $a_z = 5.5 \times 10^4 a_0$, and $a_{1D} = 2100 a_0$, where $a_{\perp,z} = (\hbar/m\omega_{\perp,z})^{1/2}$ and a_{1D} is the 1D scattering length defined in Ref. 27.

Imaging. The column densities of each state and their difference are obtained from two *in situ* phase-contrast polarization imaging (PCPI)²⁵ shots, taken in rapid succession and with different detunings near the $^2S_{1/2}$ to $^2P_{3/2}$ atomic transition. Imaging 1D gases *in situ* is problematic due to high optical densities (> 10) and heating from the first laser pulse. The first pulse dissociates atom pairs and the release of binding-energy affects the second image. At 890 G, the binding energy in 1D is $\sim 6 \mu\text{K}$, while in 3D this field corresponds to the BCS limit where there is little pairing energy. To minimize heating effects in the second image we use PCPI imaging with large detuning and low intensity for the first probe pulse, and short intervals (28 μs) between images (See supplementary information for more imaging details).

Temperature. An effective temperature is measured by fitting finite-temperature Thomas-Fermi distributions to clouds prepared with $P = 0$ ^{12,26}. Before turning on the lattice, the effective temperature is $\sim 0.05 T_F$ in the shallow trap, where T_F is the Fermi temperature of a non-interacting gas of N_1 fermions¹². As a check that the lattice turn-on is adiabatic, we turn the lattice on as described previously, wait 100 ms and turn the lattice off again by rotating the LCVR settings to trap configuration while maintaining the high laser intensity needed for the lattice. The effective temperature after this round-trip is $\sim 0.09 T_F$ in the deep trap indicating that the increase in entropy from loading the lattice is reasonably low.

Description of the spin imbalanced attractive 1D gas. Sufficiently far on the attractive side of the confinement induced resonance (CIR)²⁷, the one dimensional spin-

imbalanced attractively interacting Fermi gas may be described by the exactly solvable Gaudin-Yang model²⁸⁻³⁰ with Hamiltonian

$$H = \sum_{\sigma=1,2} \sum_{i=1}^{N_{\sigma}} \frac{p_{i\sigma}^2}{2m} + g_{1D} \sum_{i=1}^{N_1} \sum_{j=1}^{N_2} \delta(z_{i1} - z_{j2}),$$

where the 1D coupling constant is related to the 1D scattering length by $g_{1D} = -\frac{\hbar^2}{ma_{1D}}$. An energy scale is given by the two body binding energy $\varepsilon = \frac{\hbar^2}{ma_{1D}^2}$.

To obtain the equation of state at a finite temperature $t = k_B T / \varepsilon$ (from now on we put $\varepsilon = 1$) we numerically solve a truncated set of the thermodynamic Bethe ansatz (TBA) equations^{9,29}, given by two nonlinear integral equations

$$\varepsilon(k) = 2(k^2 - \mu - \frac{1}{4}) + \frac{t}{\pi} \int_{-\infty}^{\infty} \frac{dq}{1 + (k-q)^2} \ln(1 + e^{-\varepsilon(k)/t}) + \frac{2t}{\pi} \int_{-\infty}^{\infty} \frac{dq}{1 + 4(k-q)^2} \ln(1 + e^{-\kappa(q)/t})$$

$$\kappa(k) = k^2 - \mu - h + \frac{2t}{\pi} \int_{-\infty}^{\infty} \frac{dq}{1 + 4(k-q)^2} \ln(1 + e^{-\varepsilon(k)/t})$$

where $\mu = \frac{\mu_1 + \mu_2}{2}$, $h = \frac{\mu_1 - \mu_2}{2}$. Densities $n_{1,2}$ are obtained from the solution of two coupled linear integral equations²⁹ (similar to the equations for the zero-temperature Bethe ansatz)

$$(1 + e^{\varepsilon(k)/t})\sigma(k) = \frac{1}{\pi} - \frac{1}{\pi} \int_{-\infty}^{\infty} \frac{dq\sigma(q)}{1 + (k-q)^2} - \frac{2}{\pi} \int_{-\infty}^{\infty} \frac{dq\rho(q)}{1 + 4(k-q)^2}$$

$$(1 + e^{\kappa(k)/t})\rho(k) = \frac{1}{2\pi} - \frac{2}{\pi} \int_{-\infty}^{\infty} \frac{dq\sigma(q)}{1 + 4(k-q)^2}$$

as

$$n_2 a_{1D} = 2 \int_{-\infty}^{\infty} dk \sigma(k)$$

$$(n_1 - n_2)a_{1D} = 2 \int_{-\infty}^{\infty} dk \rho(k).$$

This truncation is accurate when thermal fluctuations are unable to break the tightly bound pairs, i.e. when $k_B T / \varepsilon \ll 1$ (for a detailed discussion of a similar approximation see Ref. 31). In the experiment, $k_B T / \varepsilon \approx 0.02$, and we have explicitly checked higher order terms in the TBA equations, and seen that they are small. Confinement effects³²⁻³⁴ can modify the interactions between pairs and excess fermions in a way not captured by the Gaudin-Yang model. These effects are important close to the CIR and on the repulsive side of the resonance, but are irrelevant here.

Calculation of density profiles. For each tube, we use the Thomas-Fermi local density approximation to calculate the 1D density profiles, but allow the chemical potential to vary arbitrarily from one tube to the next

$$n_{\sigma}^{1D}(\rho, z) = n_{\sigma}^{1D}(\mu^c(\rho) - \frac{1}{2} m \omega_z^2 z^2, h(\rho), t),$$

where $\sigma = 1, 2$. $\mu^c(\rho)$, $h(\rho)$ are related to the particle numbers for a tube a distance ρ from the central axis by

$$N_{\sigma}(\rho) = \int_{-\infty}^{\infty} dz n_{\sigma}^{1D}(\mu^c(\rho) - \frac{1}{2} m \omega_z^2 z^2, h(\rho), t).$$

Numerically inverting this equation, we find the central chemical potentials $\mu^c(\rho)$, $h(\rho)$. $N_{\sigma}(\rho)$ is obtained from the experimental data by inverse Abel transforming the radial profiles

$$n_{r,\sigma}(y) = \int_{-\infty}^{\infty} dz n_{c,\sigma}(y, z) = \frac{4}{\lambda^2} \int_{-\infty}^{\infty} dx N_{\sigma}(\sqrt{x^2 + y^2}) \text{ through}$$

$$N_{\sigma}(\rho) = \frac{-\lambda^2}{4\pi} \int_{\rho}^{\infty} dy \frac{\partial_y n_{r,\sigma}(y)}{\sqrt{y^2 - \rho^2}},$$

where $n_{c,\sigma}(y, z) = \frac{4}{\lambda^2} \int_{-\infty}^{\infty} dx n_{\sigma}^{1D}(\sqrt{x^2 + y^2}, z)$ is the column density. We fit the

radial densities $n_{r,\sigma}(y)$ to a simple functional form, and analytically perform the integrals. We use the extracted $N_{\sigma}(\rho)$ to normalize our radii in Fig. 3.

27. Bergeman, T., Moore, M. G. & Olshanii, M. Atom-Atom Scattering under Cylindrical Harmonic Confinement: Numerical and Analytic Studies of the Confinement Induced Resonance. *Phys. Rev. Lett.* **91**, 163201 (2003).
28. Gaudin, M. Un systeme a une dimension de fermions en interaction. *Phys. Lett. A* **24**, 55–56 (1967).
29. Yang, C. N. Some Exact Results for the Many-Body Problem in one Dimension with Repulsive Delta-Function Interaction. *Phys. Rev. Lett.* **19**, 1312–1315 (1967).
30. Takahashi, M. One-Dimensional Electron Gas with Delta-Function Interaction at Finite Temperature. *Prog. Theor. Phys.* **46**, 1388–1406 (1971).
31. Zhao, E., Guan, X.-W., Liu, W. V., Batchelor, M. T. & Oshikawa, M. Analytic Thermodynamics and Thermometry of Gaudin-Yang Fermi Gases. *Phys. Rev. Lett.* **103**, 140404 (2009).
32. Mora, C., Egger, R., Gogolin, A. O. & Komnik, A. Atom-Dimer Scattering for Confined Ultracold Fermion Gases. *Phys. Rev. Lett.* **93**, 170403 (2004).
33. Baur, S. K., Shumway, J. & Mueller, E. J. FFLO vs Bose-Fermi mixture in polarized 1D Fermi gas on a Feshbach resonance: a 3-body study. Preprint at <http://arxiv.org/abs/0902.4653> (2009).
34. Heidrich-Meisner, F., Feiguin, A. E., Schollwoeck, U. & Zwerger, W. The BCS-BEC crossover and the disappearance of FFLO-correlations in a spin-

imbalanced, one-dimensional Fermi gas. Preprint at

<http://arxiv.org/abs/0908.3074> (2009).

Supplementary information

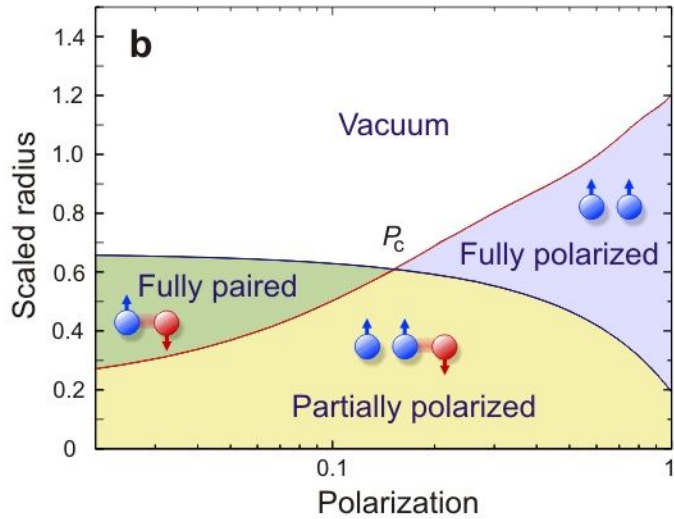
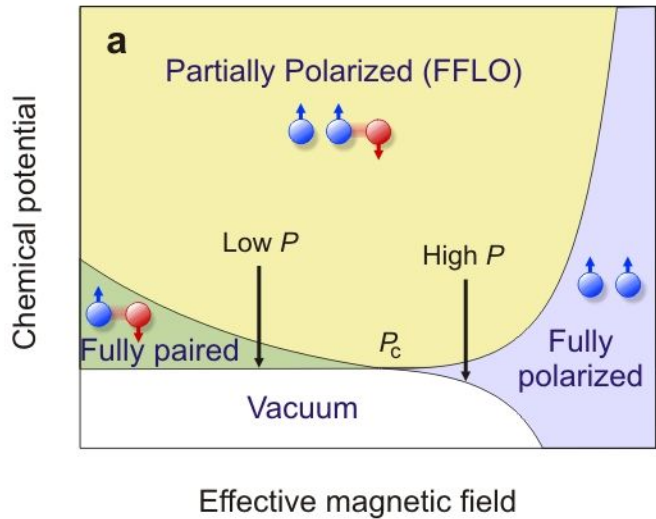
Imaging. We use polarization phase contrast imaging, as illustrated in Fig. S1. The first probe pulse is detuned to the red of the state $|2\rangle$ transition by 15Γ , where $\Gamma = 5.9$ MHz. This corresponds to a red detuning from the state $|1\rangle$ transition of 28Γ since states $|1\rangle$ and $|2\rangle$ are separated by 76 MHz (see Fig. S1b). The second laser pulse is tuned in between the state $|1\rangle$ and $|2\rangle$ transitions. The intensity of the first probe pulse is low to minimize heating, while the intensity of the second is higher to improve the signal-to-noise ratio. Both phase contrast images are linear combinations of the two states with different weighting factors: the first image involves a sum, while the second shot is the difference (see Fig. S1c for an example). The two images are deconvolved to obtain column density images of $|1\rangle$ and $|2\rangle$. The imaging resolution of $\sim 4\ \mu\text{m}$ is insufficient to resolve individual 1D tubes separated by $\lambda/2 = 0.5\ \mu\text{m}$.

Figure S1: The imaging process. **a**, The PCPI imaging setup. The linearly polarized probe beam is made circularly polarized by the quarter wave plate (left). The light coherently scattered by the atoms is elliptically polarized, which is analyzed by a polarizer (right) whose polarization axis is at a 15° angle to the original polarizer. The image is recorded by a CCD array camera. **b**, The relevant energy levels and probe beam frequencies. The first probe S1 is detuned $\Delta = 15\Gamma$ from state $|2\rangle$, and the second probe S2 is tuned half way between states $|1\rangle$ and $|2\rangle$. **c**, Column density images from probes S1 and S2 corresponding to global $P = 0.61$. **d**, Column density profiles of state $|1\rangle$ and $|2\rangle$, and their difference deconvolved from images S1 and S2.

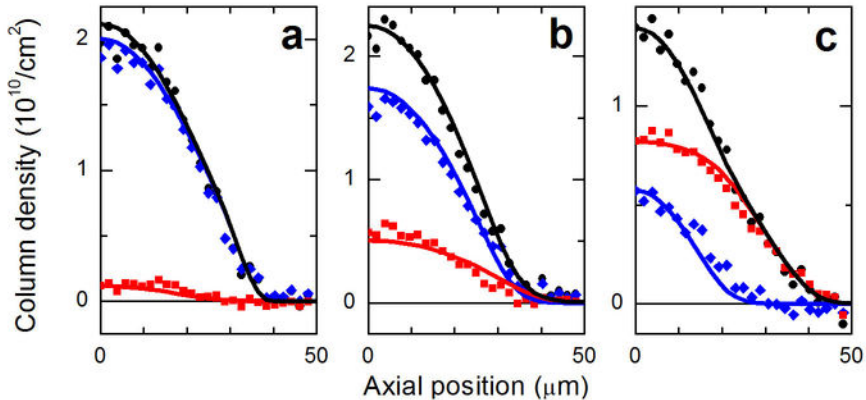
Figure 1: Theoretical $T = 0$ phase diagram. **a**, Schematic with μ vs. h showing three phases: fully paired (green), fully polarized (blue), and partially polarized (yellow) that is predicted to be FFLO. In a trap, μ decreases from the centre to the edge, while h is constant throughout the tube. The vertical arrows show two possible paths from trap centre to edge: The partially polarized centre is surrounded either by a fully paired superfluid phase at low h or by a fully polarized phase at high h . At a critical value of h , corresponding to a polarization P_c , the whole cloud is partially polarized. **b**, Phase diagram of the trapped gas. The scaled axial radius is defined in the Fig. 3 caption. The red line corresponds to the scaled radius of the density difference, while the blue line is the scaled radius of state $|2\rangle$.

Figure 2: Column density profiles of a spin-imbalanced 1D ensemble of tubes. Column density profiles (black: majority; blue: minority; red: difference) are shown as function of P . Lines are theoretical predictions from the finite temperature thermodynamic Bethe ansatz (130 nK) within the local density approximation, using the measured radial 3D density distribution as input. **(a-c)** P corresponds to 0.05, 0.15, and 0.59, respectively. **a**, At low P , the edge of the cloud is fully paired and the density difference is zero. **b**, Near P_c , nearly the entire cloud is partially polarized. **c**, Well above P_c , the edge of the cloud becomes fully polarized and the minority density is zero. These column density profiles are averaged over a radial distance of $9.4 \mu\text{m}$.

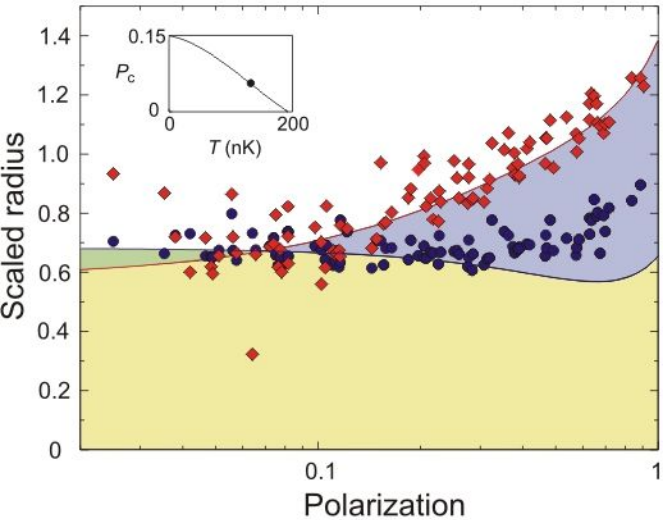
Figure 3: Experimental phase diagram as a function of polarization in the central tube. The scaled radius of the density difference (red diamonds) and state $|2\rangle$ density (blue dots) are compared with Bethe ansatz calculation for $T = 130$ nK (solid lines). For the central tube, $T_F = 1.25$ μ K (see Methods). The dimensionless scaled radius, $R_{\text{scaled}} = R/(N_0^{1/2} a_z)$, where R is the central tube axial radius, N_0 is total number in the central tube, and a_z is the axial harmonic confinement length. At $P \sim 0.07$, both radii intersect indicating that the entire cloud is partially polarized. The inset shows how P_c varies with T .



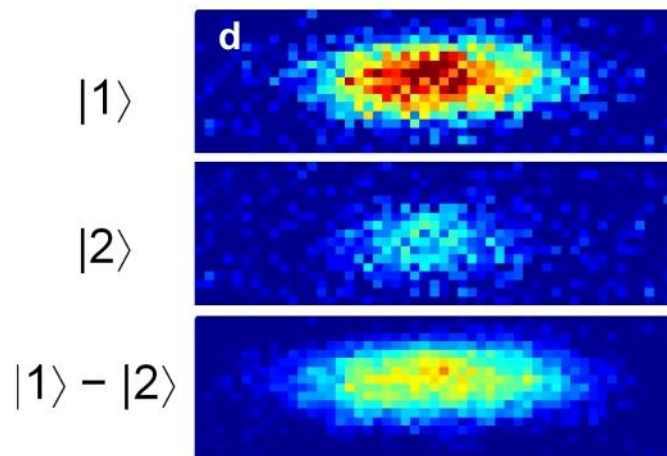
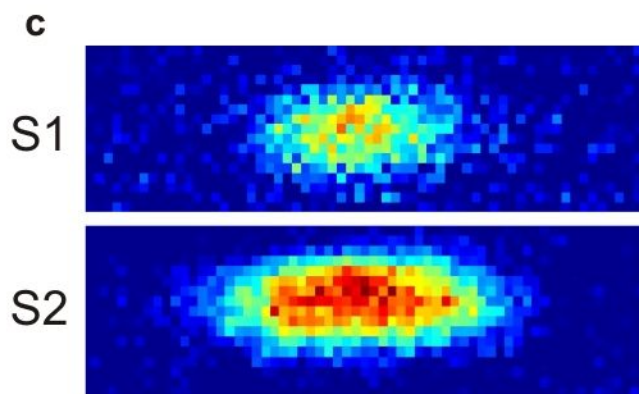
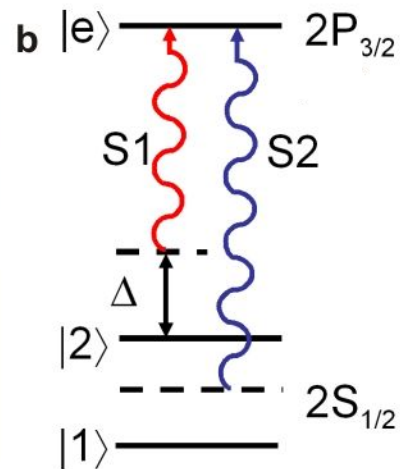
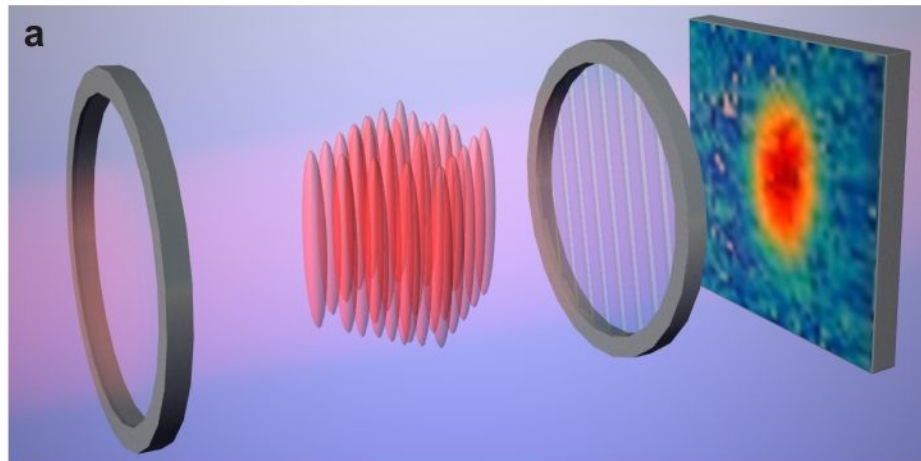
Author: Liao *et al.*
Figure 1



Author: Liao *et al.*
Figure 2



Author: Liao *et al.*
Figure 3



Author: Liao *et al.*
Figure S1